Electrochimica Acta 65 (2012) 57–63

Contents lists available at SciVerse ScienceDirect

Electrochimica Acta

journal homepage: www.elsevier.com/locate/electacta

Formation of a silicon layer by electroreduction of SiO_2 nanoparticles in $CaCl_2$ molten salt

Sung Ki Cho, Fu-Ren F. Fan, Allen J. Bard *

Center for Electrochemistry, Department of Chemistry and Biochemistry, 1 University Station A5300, The University of Texas at Austin, Austin, TX 78712, United States

ARTICLE INFO

Article history:
Received 19 October 2011
Received in revised form 4 January 2012
Accepted 4 January 2012
Available online 13 January 2012

Keywords:
Photovoltaic
Silicon oxide
Electrochemistry

ABSTRACT

We observe the electrochemical formation of a silicon layer on a molybdenum (Mo) electrode at 850 °C in a $CaCl_2$ melt containing silicon oxide (SiO_2) nanoparticles (NPs). A stable electrochemical cell for high temperature molten salt was fabricated from a sealed quartz tube, with a glassy carbon counter electrode and a Ca/Ca^{2+} dynamic reference electrode. When SiO_2 NPs are added into the $CaCl_2$ melt, the reduction current and the generation of a new redox couple relating to the reduced silicon were observed in a cyclic voltammogram at Mo. Spectroscopic analyses confirmed the formation of a silicon layer from the reduction of SiO_2 NPs. Although the deposit was not continuous, XPS shows that it is silicon of good purity and XRD shows the pattern of crystalline silicon. We also investigated the dissolved silicon species generated after the oxidation of electrodeposited silicon in $CaCl_2$ melt, which produces a redox couple at potentials positive of the deposition potential. We tentatively attribute it to the oxidation and re-reduction of an insoluble Si–Cl surface species.

1. Introduction

Currently there is a high demand and consumption of silicon as a material for photovoltaic (PV) devices. Most photovoltaic devices are based on the crystalline silicon p-n junction, and accordingly, the price of silicon has a great effect on the cost of these devices. The purity of silicon required for photovoltaic devices, which is called 'solar silicon', is 99.9999% (6N), which is less pure than that for electronics applications (11N). There is therefore a strong interest in developing a low cost production processes for solar silicon, compared to conventional high purity silicon production process such as the Siemens process, especially a process that can produce thin films of needed purity and crystallinity directly. Generally, high purity silicon is produced by the carbothermic reduction of SiO_2 with carbon at 2000 °C followed by the purification with HCl at 1000 °C. These processes are highly energy-consuming with considerable emission of CO_2.

Electrochemical approaches for producing silicon have been studied; these are attractive because they could lead to a less expensive route to solar Si. In general electrochemical apparatus is simpler than that for vacuum processes and it is easier to control the process variables [1]. Since the Si/SiO_2 couple has a very negative potential for reduction and Si can be easily oxidized, the electrochemical formation of silicon is usually carried out in non-aqueous solution. Many studies [2–8] on silicon electrodeposition have been carried out in organic solvents or room temperature ionic liquids, where silicon halide compounds such as $SiCl_4$ and $SiHCl_3$ are usually used as precursors. However, the silicon deposits obtained were coarse and impure. Moreover, the silicon was so porous that it was easily oxidized, and so far, has been unsuitable for use as solar silicon. Another choice for electrolyte for depositing silicon is a high temperature molten salt [9–15]. $LiF/KF/K_2SiF_6$ (at 745 °C) has been investigated and is said to be capable of growing relatively pure (up to 4N) crystalline silicon. However there are issues about the low deposition rate, which is an important consideration in a manufacturing process and the safety in handling fluoride compounds [9–11,15]. It is also possible to make silicon from alkali or alkaline earth silicate melts such as $BaO–SiO_2–BaF_2$ and $SrO–SiO_2–SrF_2$ (at 1465 °C) [12–15]. The extremely high operating temperature results in high-energy consumption and leads to liquid silicon formation, which is mixed with the melt and makes it difficult to separate.

More recently, Nohira et al. [16,17] reported that solid SiO_2 can be electrochemically reduced to crystalline silicon in a calcium chloride melt. In a $CaCl_2$ melt, electrons can be transferred from a metal (molybdenum, tungsten, nickel) cathode directly to a mechanically contacted solid quartz piece. The reduction reaction starts at metal/electrolyte/metal oxide three-phase interface and the oxygen ion is removed from the solid structure.

$$SiO_2(s) + 4e^- \rightarrow Si(s) + 2O^{2-} \quad (1)$$

* Corresponding author. Tel.: +1 512 471 3761; fax: +1 512 471 0088.
E-mail addresses: ajbard@mail.utexas.edu, asn@mail.utexas.edu (A.J. Bard).

0013-4686/$ – see front matter © 2012 Elsevier Ltd. All rights reserved.
doi:10.1016/j.electacta.2012.01.008

This seems to be a promising approach, because silicon dioxide is a cheap and abundant source material and the operating conditions are less severe than those for other molten salt systems. In this study, we show that one can produce a silicon layer on Mo surface from SiO_2 NPs simply added into the $CaCl_2$ melt. We performed cyclic voltammetry for this reaction in the $CaCl_2$ melt, and also characterized the silicon deposit by SEM-EDS, XRD and XPS. However, the deposit still is not of sufficient quality to be useful for solar applications.

2. Experimental

2.1. Apparatus and equipment

Experiments were performed in a quartz tube electrochemical cell; a schematic diagram is shown in Fig. 1. A 40 cm long quartz tube (5 cm dia.) with one open end was closed with a 316 stainless steel cap, using an O-ring and clamp. The stainless steel cap has electrode feedthroughs and in- and outlet valves for Ar gas. The electrode feedthroughs were fabricated with 316 stainless steel tube fittings (Swagelok, Essex Junction, VT) combined with 0.1 cm dia. 304 stainless steel wires, which were coated with heat shrinkable Teflon tubes (Zeus, Gaston, SC) to insulate electrodes from the tube fittings. The working electrode feedthrough was made of stainless steel wire with a rubber stopper that facilitates the vertical movement of the electrode inside the closed tube cell. This made it possible to maintain the electrode above the molten salt and only insert the electrode into the $CaCl_2$ after it melted and to remove the electrode from the melt after the electrochemical reaction is finished and hold it in the inert atmosphere. All connecting points on feedthroughs were covered with vacuum seal (Varian, Milpitas, CA) to prevent air from entering the cell. Ar gas was fed into the cell through a 20 cm long 304 stainless steel tube, which was connected with a stainless steel ball valve (Swagelok, Essex Junction, VT) and was vented via a stainless steel bleed valve (Swagelok, Essex Junction, VT). All electrodes were connected to the feedthroughs via homemade nickel line connectors and a nickel clamp. The quartz tube assembled with a stainless steel cap was inserted into the vertical tube furnace (21100, Barnstead/Thermolyne, Dubuque, IA)

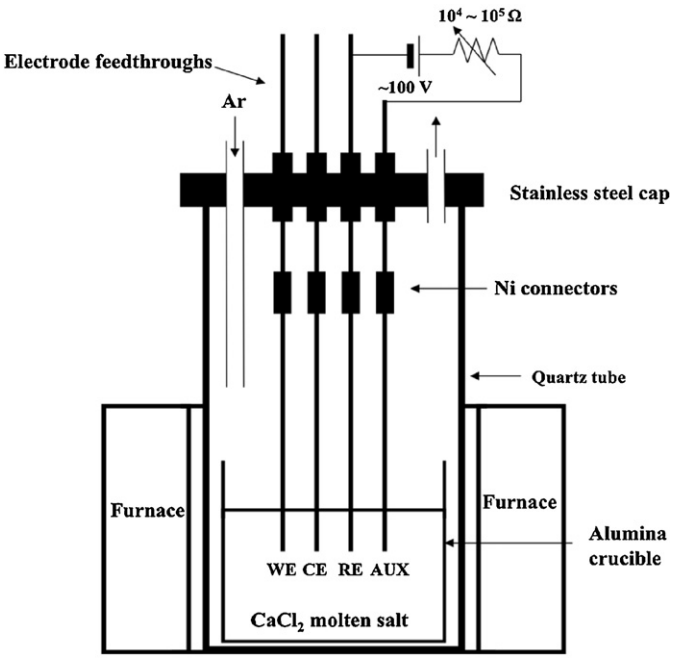

Fig. 1. Schematic diagram of experimental apparatus used in this study.

and heated to 850 °C at increments of 10 °C/min. Electrochemical analyses were performed under argon gas (99.9995%, Praxair, Inc., Danbury, CT) over the melt.

2.2. Materials and chemicals

Calcium chloride dihydrate ($CaCl_2{\cdot}2H_2O$, ≥99%, Sigma–Aldrich, St. Louis, MO), used as the electrolyte, was dried in vacuum at 200 °C for over 6 h to remove water in $CaCl_2$, bound chemically and physically [18]. A sample of 32.5 g was then placed in a 3.5 cm outer dia. cylindrical alumina crucible (99.8% Al_2O_3, Fisher Scientific, Pittsburgh, PA) at the bottom of a quartz tube in a furnace. The silicon precursor used in this study was colloidal silicon dioxide (SiO_2, 5–15 nm, 99.5%, Sigma–Aldrich, St. Louis, MO). The working electrode was a Mo wire (1 mm dia., 99.94%, Alfa Aesar, Ward Hill, MA) or Mo foil (0.3 cm wide and 0.025 cm thick, 99.94%, Alfa Aesar, Ward Hill, MA). N-type (1 0 0) silicon wafers (As-doped, 0.003 Ω/sq., 0.3 cm wide and 400 μm thick, University Wafer, Boston, MA) were also used as working electrodes. The counter electrode was glassy carbon (GC, 0.3 cm dia., Alfa Aesar, Ward Hill, MA) or a graphite rod (0.25 cm dia., Alfa Aesar, Ward Hill, MA).

2.3. Electrochemical analysis

The choice of reference electrode is not trivial for electrochemistry in high temperature molten salts. In this study, we used a dynamic Ca/Ca^{2+} reference electrode. This was made by cathodically polarizing a Mo wire with respect to an auxiliary electrode by connecting it to a battery (to prevent interaction with the potentiostat) and a resistor, as shown in Fig. 1, to continually generate Ca at a current density of about 10 mA/cm^2 [19]. By controlling this current, we can define and fix the potential of the reference electrode. A few previous studies have used dynamic reference electrodes in high temperature molten salts [20–22]. In the $CaCl_2$ melt, the reduction of calcium ion occurs on the cathodically polarized Mo electrode, and chlorine gas is generated on the carbon auxiliary electrode. The adjustable resistor used in this study was in the range of 10^4–10^5 Ω, which is much higher than the resistance of the $CaCl_2$ melt and the reaction resistance of the Ca^{2+} reduction, and therefore the current passing through the Mo electrode is determined by this resistor. The current on the Mo electrode was monitored with a multimeter by measuring the potential drop across the resistor. The dynamic reference electrode was stable for more than 8 h within ±5 mV. When the $CaCl_2$ melts containing SiO_2 NPs were used, the reference electrode was a graphite quasi-reference electrode, and all potentials were later calibrated and are reported with respect to the Ca/Ca^{2+} dynamic reference electrode.

Cyclic voltammetry and constant current electrolysis were carried out with an Eco Chemie Autolab PGSTAT30 potentiostat (Utrecht, Netherlands). The length of the working electrode immersed in the electrolyte was 0.7 cm. After the experiments were finished, the whole cell was cooled slowly (~2 °C/min) under Ar flow and the electrode was cleaned and sonicated in water.

2.4. Spectroscopic analysis

The Si deposit was examined with a scanning electron microscope (SEM, Quanta 650 FEG, FEI Company, Inc., Hillsboro, OR). The composition and crystallinity of the Si deposit were characterized by energy dispersive spectroscopy (EDS) (XFlash® Detector 5010, Bruker, Fitchburg, WI), X-ray photoelectron spectroscopy (Kratos XPS, Kratos Analytical Ltd, UK) equipped with a monochromatic Al X-ray source, and X-ray diffractometry (XRD) with a D8 ADVANCE (Bruker, Fitchburg, WI) equipped with a Cu Kα radiation source. In the case of XPS, a specimen could be loaded in the XPS chamber without exposing the specimen to air. After the electrochemical

reaction, the specimen was removed from the $CaCl_2$ melt by pulling up the stainless steel feedthrough in the rubber stopper, and cooled slowly under an Ar atmosphere. Then, the whole cell was put into the Ar-filled glove box (Vacuum Atmospheres Corp., Hawthorne, CA) and the specimen was removed from the cell. Solidified $CaCl_2$ residue was removed by dipping the specimen in hydrazine (anhydrous, 98%, Sigma–Aldrich, St. Louis, MO), in which $CaCl_2$ is highly soluble [23]. The specimen was cleaned further with propylene carbonate (anhydrous, 99.7%, Sigma–Aldrich, St. Louis, MO) and was dried on a hot plate at 40 °C. Finally it was transferred to the XPS chamber for analysis using a homemade airtight kit, which can load the specimen into the XPS chamber without air exposure.

3. Results and discussion

3.1. Cyclic voltammetry at Mo electrode in $CaCl_2$ melt in the absence of SiO_2 NPs

Fig. 2 shows cyclic voltammograms (CVs) and chronopotentiograms (CPs) on a Mo electrode in $CaCl_2$ melt, with potential, E, vs. a Ca/Ca^{2+} dynamic reference electrode. Mo is an exceptionally stable material at high temperature, so it is frequently used as a working electrode in electrochemical studies in molten salts. The CVs on Mo show that almost no reaction occurs in the negative potential region prior to the onset of reduction current for the reduction of Ca^{2+}. Since the reaction at the dynamic reference electrode is also the reduction of Ca^{2+}, the current, as expected, increases sharply near 0 V and the potential for the Ca^{2+} reduction is progressively shifted positively according to the current density of the dynamic reference electrode, until the CV is only slightly dependent on the current density of the dynamic reference electrode (Fig. 2a). Even with the large reduction current observed, there is no, or only very little, re-oxidation current of the reduced Ca on a reverse scan, because Ca is a liquid (melting temperature 842 °C) at the melt temperature and soluble up to 3 mol% in a $CaCl_2$ melt [24,25]. Thus, dissolved Ca can mass transfer away from the electrode surface by convection. Strong convection in the melt due to the thermal gradient between the melt bottom and the top facing the incoming Ar gas flow probably occurs. This is consistent with the chronopotentiometric results shown in Fig. 2c. In chronopotentiometry with reversal (50 mA for reduction followed by −50 mA for oxidation) on a 0.1 cm dia. Mo wire (giving a current density of 227 mA/cm^2), only the oxidation of Mo electrode was observed in the oxidation step even though Ca was deposited at the Mo electrode in the forward step (Fig. 2c). Note that the oxidation of the Mo electrode occurs above 2 V vs. Dyn. Ca/Ca^{2+} as shown in a CV on Mo (Fig. S1 in the Supporting information). When the Mo electrode was left at open circuit after the Ca^{2+} reduction step, the electrode potential gradually recovered to that of the Mo electrode (Fig. 2c). These results indicate that Ca was removed spontaneously from the surface. The reversal oxidation peak of the Ca deposit could be observed in CV when a large amount of cathodic charge was collected by reversing the potential after a large reduction current (e.g., over 600 mA) as shown in Fig. S1 in the Supporting information. Moreover, this loss of Ca from the electrode surface due to its solubility in the melt caused a considerable shift of the Dyn. Ca/Ca^{2+} potential from $E^{o'}$ (Ca/Ca^{2+}). Supporting information Fig. S1 shows that the backward scan after Ca generation intersects the zero current x-axis at around −0.35 V, which is the equilibrium potential of Ca/Ca^{2+} with unity activity for both species. This indicates that the Dyn. Ca/Ca^{2+} potential is positively shifted by 0.35 V from $E^{o'}$ (Ca/Ca^{2+}). Generally, the potential difference between a dynamic reference electrode and a normal reference electrode is mainly caused by the dynamic reference electrode current × the uncompensated resistance, which is very small (<10 mV) because of the small current employed [19]. However, for the dynamic

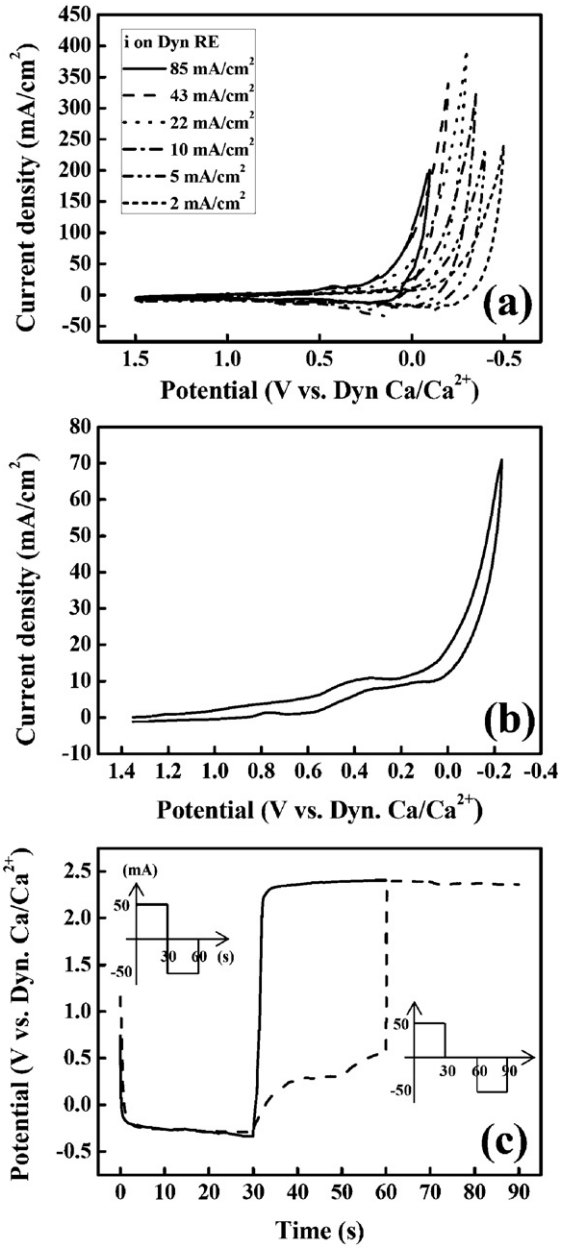

Fig. 2. Cyclic voltammogram of Mo electrode (1 mm dia. wire, 0.22 cm^2) (a) at a scan rate of 100 mV/s with different current densities passing on dynamic reference electrode (1 mm dia. Mo wire, 0.22 cm^2) and (b) at a scan rate of 20 mV/s (with 10 mA/cm^2 passing on dynamic reference electrode), and (c) chronopotentiogram of Mo electrode (1 mm dia., 0.22 cm^2) with the current steps in 850 °C $CaCl_2$ melt.

reference electrode in this study, the activity of Ca in Dyn. Ca/Ca^{2+} is significantly smaller than one, leading to a positive shift of the potential. Therefore all reported potentials can be referenced to the Ca/Ca^{2+} electrode by adding 0.35 V. Upon increasing the current sensitivity as shown in Fig. 2b, we observed small redox peaks near 0.5 V vs. Dyn. Ca/Ca^{2+}, which are presumed to be related to the formation and removal of a Mo-Ca phase. Note, however that the presence of convection within the melt suggests that little useful information about products can be obtained from reversal experiments, except when products are insoluble or irreversibly adsorbed on the electrode.

3.2. Electrochemical reduction of SiO_2 NPs on Mo in $CaCl_2$ melts

The addition of SiO_2 NPs to the $CaCl_2$ melt led to the change in CV on a Mo foil electrode (Fig. 3). The increase in the reduction current

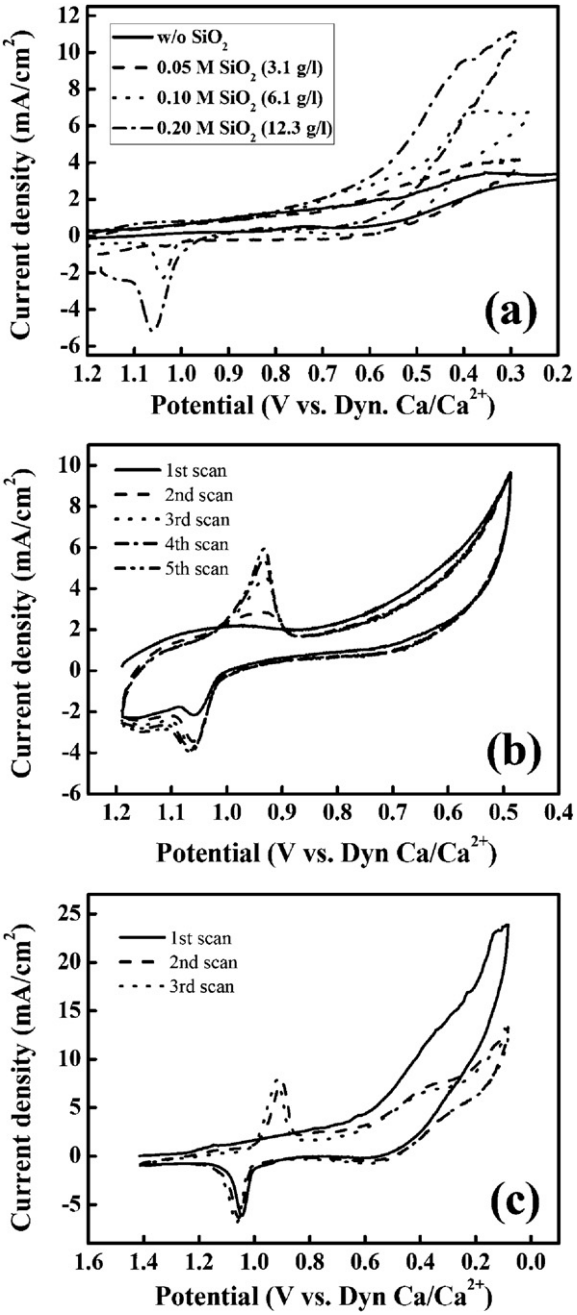

Fig. 3. Cyclic voltammograms of Mo foil (0.3 cm width, 0.42 cm^2) (a) with different concentrations of SiO_2 nanoparticles in 850 °C $CaCl_2$ melt, and (b and c) with the multiple scans in 850 °C $CaCl_2$ melt containing 0.2 M SiO_2 at a scan rate of 20 mV/s.

starts at ~0.8 V vs. Dyn. Ca/Ca^{2+}, which rises to a current density of about 5 mA/cm^2 at about 0.5–0.6 V (Fig. 3a), considerably before the reduction of Ca^2. Note that all bulk electrolyses were carried out at potentials positive of the Ca^{2+} reduction potential, so direct reduction of SiO_2 by dissolved Ca was avoided. The potential for reduction of SiO_2 as estimated is similar to the value reported in the literature on the reduction of a solid quartz piece [26,27]. We attribute this to the reduction of SiO_2 (Eq. (1)). Contrary to the usual electrodeposition process, this is not a reaction of dissolved SiO_2, because it is insoluble in the $CaCl_2$ melt, but rather from colloidal SiO_2. In spite of the insolubility of the SiO_2 NPs, the reduction current still depended on the SiO_2 concentration, as illustrated in Fig. 3a. As observed in a solid phase reaction, the process involved here might consist of (1) mass transfer or adsorption of SiO_2 to the Mo surface, (2) electron transfer to the SiO_2 NPs, and (3) mass transfer of oxide ion from the SiO_2 NPs with some surface processes such as the surface diffusion, nucleation, and coalescence of silicon. As mentioned earlier, an exact treatment of the mass transfer of the SiO_2 NPs in the high temperature $CaCl_2$ melt is difficult because the unfavorable electrode geometry and the unknown convection. Moreover, the size distribution of the particles in the melt is not known. In general, the limiting current (i_l) of the reduction controlled by the mass transfer of reactant can be expressed as:

$$i_l = nFAmC \quad (2)$$

where n is the number of electron involved, and F is faraday constant, and A is the surface area (0.42 cm^2), m is the mass transfer coefficient, and C is the concentration of the reactant. When the NPs move to the electrode and are reduced, the current can be estimated by Eq. (2). The concentration of SiO_2 added here is about 0.2 M (in terms of moles Si) which corresponds to $\sim 1.6 \times 10^{-5}$ M in terms of the concentration of NP, since each SiO_2 NP contains about thirteen thousand SiO_2 molecules. When a large mass transfer coefficient (e.g., 10^{-2} cm/s) is assumed for the convection, the reduction current can be roughly estimated as ~30 μA assuming only 4 electrons transferred to NP; this is much smaller than the actual value (~4 mA) estimated at 0.4 V vs. Dyn. Ca/Ca^{2+}. The currents shown in Fig. 3a are approximately proportional to the concentration of SiO_2 NP and show a steady value consistent with convection. The best explanation of the observed current is that the effective number of electrons for the reduction of a given SiO_2 NP is very large, e.g. about 600, implying that a few hundred SiO_2 molecules in a single NP are reduced when it collides with the electrode (and probably sticks). Similar effects have been observed for IrO_x NPs, where all of the centers are accessible in a particle [28]. However, the effective number of electrons is only a fraction of the estimated number of molecules in each NP, and the curves of the reduction currents in all CVs show a gentle slope, suggesting that the reduction reaction is kinetically slow. Since SiO_2 is an insulator (its resistivity is around 10^9 Ω cm at 900 °C) [29] and the Si forms a solid film, the rate of electron transfer from Mo to SiO_2 and the escape of oxygen ion from SiO_2 structure could be kinetically very slow for some forms of SiO_2. This is probably the reason why many papers dealing with the electroreduction of a larger quartz piece or a silicon dioxide pellet report the requirement of a long electrolysis time and the difficulty for the complete conversion to elemental Si [16,17,30]. This reaction should be much easier and faster with NPs relative to a piece of bulk quartz, but the heterogeneous kinetics for the reduction could still be the rate-determining step.

Following the reduction wave, on scan reversal, an oxidation peak appears at around 1.05 V vs. Dyn. Ca/Ca^{2+} in the CV. This peak is about 0.4 V positive of the reduction wave for SiO_2. After scanning over this oxidation wave, a new reduction peak appears on reversal, which was not present in the initial scan and is clearly connected to the oxidation peak in multi-cycle CV. The peak heights of this redox couple built up gradually with repeated scans (Fig. 3b) and appear to be related to the oxidation and re-reduction of silicon formed during the CV. When the electrode was scanned further negative, the reduction current of SiO_2 decreased in the next scan (Fig. 3c), since the electrode surface was gradually covered by silicon, which forms a resistive layer on the Mo. The passivation of the electrode by silicon deposit has also been observed in silicon electrodeposition from an organic solvent [8]. Because of the strong convection in the molten salt, reversal waves signal surface species rather than products diffusing away from the electrode. Thus the redox peaks observed in the potential range of 0.9–1.1 V (Fig. 3b and c) can be attributed to a surface electrochemical reaction and their areas are essentially equal, indicating the oxidized species is stable. The position of the new re-reduction peak is less negative than that for SiO_2 reduction. Further electrochemical analyses by the scan rate

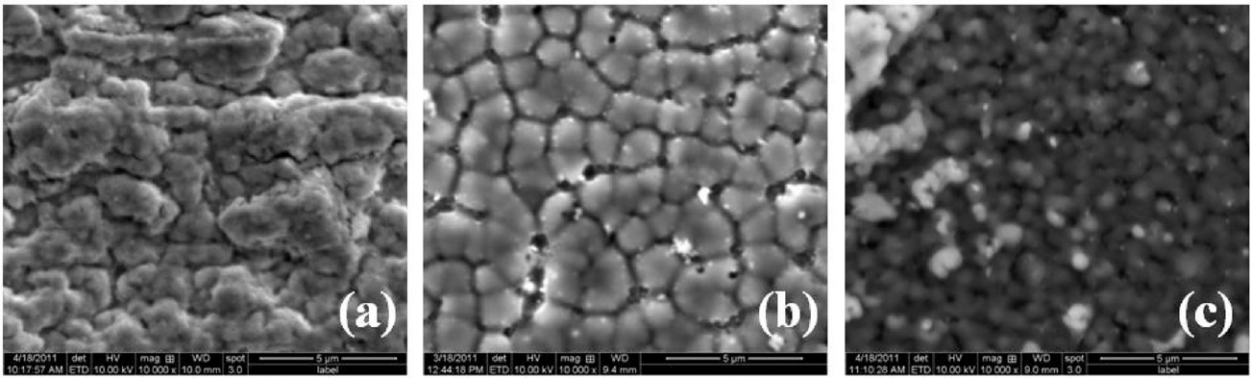

Fig. 4. SEM images of Si deposited on (a) Mo, (b) n-type Si wafer, and (c) glassy carbon. Si was deposited at 0.45 V vs. Dyn. Ca/Ca^{2+} for (a) 3000 s, (b) 2000 s, and (c) 1500 s in 850 °C $CaCl_2$ melt containing 0.2 M SiO_2 nanoparticles. EDS analyses shows that the films are composed of (a) Si 43 at.%, O 3 at.%, C 11 at.%, and Mo 43 at.%, (b) Si 88 at.%, O 1 at.%, and C 11 at.%, and (c) Si 34 at.%, O 58 at.%, and C 8 at.%, respectively.

dependency of the CV peak and chronoamperometry are essential for a more detailed mechanistic study on the reduction of SiO_2, but we have been unable to prepare a useful ultramicroelectrode or a rotating disk electrode for quantitative electrochemical analyses in the high temperature molten salt.

The same CV behavior, irreversible reduction current and the formation of a new redox couple, was also observed with a Mo electrode contacting or wrapped around a piece of quartz or in a $CaCl_2$ melt containing sodium silicate (Na_2SiO_3) powder (Fig. S2 in the Supporting information). The reduction of quartz into silicon powder was reported in several papers [16,17,30], and we also found that sodium silicate can also be used as a Si precursor in a $CaCl_2$ melt. Since silicate is composed of a chain polymeric anion with a SiO_4 tetrahedral structure, which is similar to that in SiO_2, a similar reaction scheme probably is valid with Na_2SiO_3 in $CaCl_2$.

3.3. Characterization of silicon deposit by SEM-EDS and XPS

SEM-EDS analysis confirmed the formation of a silicon layer from SiO_2 electroreduction in $CaCl_2$ melt. Fig. 4 shows SEM images of silicon deposited on Mo foil, an n-type silicon wafer, and glassy carbon. EDS analysis showed that the large amount of silicon (43 at.%) formed on the Mo surface with small oxygen and carbon contents. However, the deposit is granular, composed of grains a few μm size. The deposited material was not a continuous film, but was rather closer to those of previous studies of the reduction of a quartz piece or SiO_2 pellet in $CaCl_2$ [17,30,31]. The reaction from solid SiO_2 perhaps involves a small interaction with the substrate material, even with a silicon wafer, where the nucleation and surface diffusion of the deposited silicon atoms are slow, resulting in three-dimensional growth of silicon. Although the film is not continuous, it shows polycrystalline structure as shown in Fig. 5. Si (1 1 1), (3 1 1), and weak (2 2 0) crystallites were detected on a Si (1 0 0) wafer after Si growth though those peaks are small compared to the (4 0 0) peak from the substrate. The grain size of Si (1 1 1) calculated from the Scherrer equation is about 33 nm, which is much smaller than those of the granules that appear in the SEM images. This is significantly different from silicon electrodeposited at room temperature in non-aqueous solution, which generally produces amorphous silicon. The high operating temperature probably assists in silicon crystallization. Fig. 6 shows the XPS Si 2p spectrum of a silicon deposit on Mo. The strong peak at 99.5 eV corresponds to elemental silicon, with a smaller native oxide peak (103.0 eV), indicating that the electrodeposited silicon is in the elemental state. In addition to the silicon peak, a strong Mo (3d) peak was also detected on the surface, indicating that the silicon did not cover the whole

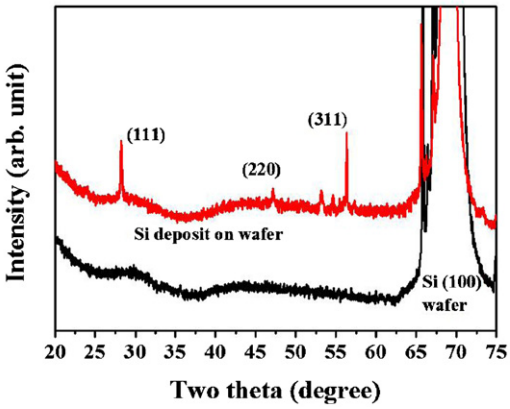

Fig. 5. θ–2θ X-ray diffraction spectrum of silicon deposit on n-type silicon (1 0 0) wafer. Si was deposited at 0.40 V vs. Dyn. Ca/Ca^{2+} for 2000 s in 850 °C $CaCl_2$ melt containing 0.2 M SiO_2 nanoparticles.

Mo surface and is somewhat porous. We attempted to measure the photo-oxidation of *N*,*N*,*N*′,*N*′-tetramethyl-*p*-phenylenediamine or the photo-reduction of ethyl viologen in acetonitrile solution under UV–vis light irradiation of a Si deposit on Mo [32]. Only very small (~10^{-6} A/cm^2) photocurrent responses were detected, which revealed that a Si deposit was not as pure as solar grade silicon. The high porosity of the Si film led to a high background current originating from a dark reaction occurring on the exposed Mo surface,

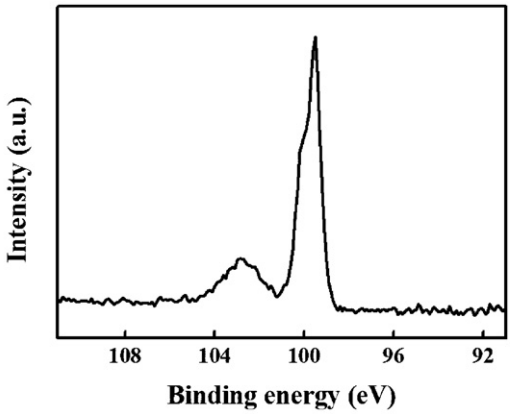

Fig. 6. X-ray photoelectron spectrum of Si 2p of silicon deposit, which was grown on Mo at 0.45 V vs. Dyn. Ca/Ca^{2+} for 2500 s in 850 °C $CaCl_2$ melt containing 0.2 M SiO_2 nanoparticles.

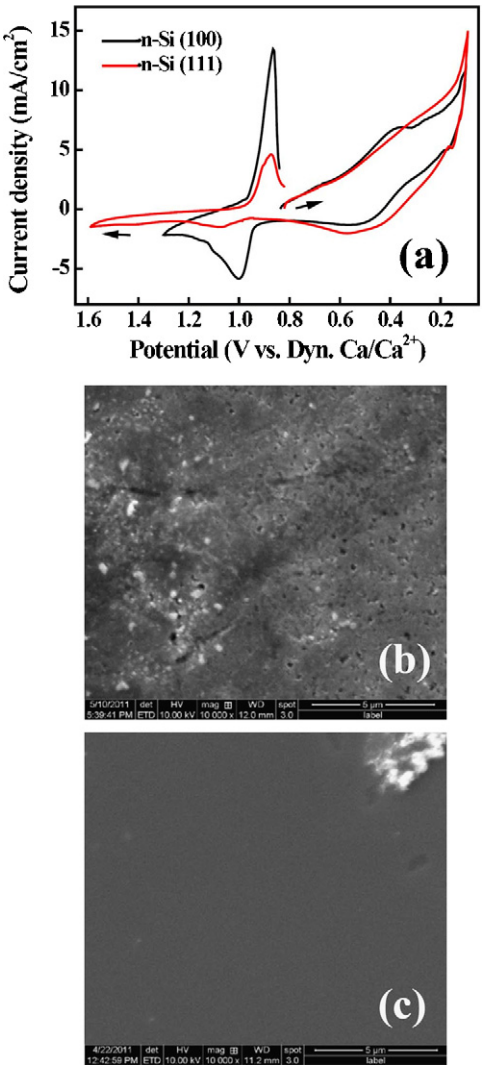

Fig. 7. (a) Cyclic voltammograms at n-type silicon (1 0 0) and (1 1 1) wafers (0.003 Ω/sq., 0.3 cm width, 0.42 cm^2) in 850 °C $CaCl_2$ melt at a scan rate of 20 mV/s, and SEM images of an n-type silicon wafer (b) oxidized at 1.2 V vs. Dyn. Ca/Ca^{2+} for 400 s, and (c) immersed (without the oxidation), in 850 °C $CaCl_2$.

which made the reliable measurement of the photocurrent even more difficult.

The silicon deposit obtained from Na_2SiO_3 (Fig. S3 in the Supporting information) morphology and composition was very similar to those obtained from SiO_2 NPs.

3.4. Electrochemistry of silicon in $CaCl_2$ melt

As discussed above, the electroreduction of SiO_2 on Mo leads to the appearance of a new pair of redox peaks in the CV. A similar redox couple was also observed with an n-type Si wafer working electrode in $CaCl_2$ melts without SiO_2 NPs (Fig. 7a). This confirms that the generation of the redox peak is due to the formation of a silicon layer on the Mo surface. The shape of the reduction peak indicates it is related to a reaction that is confined to the surface. The oxidation of a Si wafer at 1.2 V vs. Dyn. Ca/Ca^{2+} for 400 s generated pits and pores on the surface (Fig. 7b) whereas a non-oxidized wafer surface did not change in a $CaCl_2$ melt (Fig. 7c). The oxidative dissolution of an n-type Si wafer might be caused by holes created by a small amount of light (photooxidation) from the glow of the furnace, or by the increased charge carrier density at high temperature causing the Si to become degenerate and more conductive [33]. The

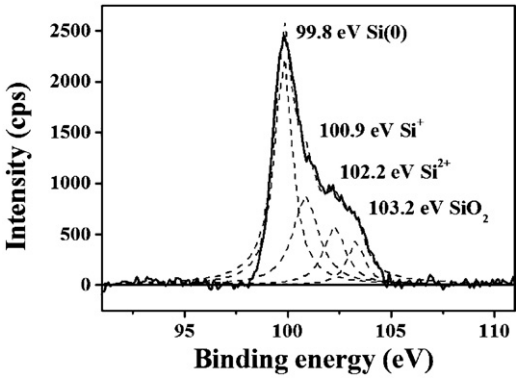

Fig. 8. X-ray photoelectron spectrum of Si 2p of an n-type silicon wafer (0.003 Ω/sq.) oxidized at 1.2 V vs. Dyn. Ca/Ca^{2+} for 600 s in 850 °C $CaCl_2$ melt.

anodic oxidation and dissolution of silicon in HF solutions has been widely investigated [34–38] and the dissolution rate, expressed as a current density, can be as high as a few tens to 100 mA/cm^2 or more with increasing applied potential. On the other hand, the oxidation of a Si wafer in a $CaCl_2$ melt showed a relatively small current peak followed by a small limiting current as shown in the CV (Fig. 7a). Analogous silicon dissolution phenomena are observed in alkaline solutions such as KOH and NaOH [34,35,39–41]. In these media passivation of the surface with OH-terminated silicon prevents fast dissolution and produces a small oxidation peak in CV with the peak height less than 1 mA/cm^2, which is related to the number of active silicon sites exposed to the electrolyte. OH-terminated silicon is slowly converted to $Si–2OH_{ads}$ and $Si–3OH_{ads}$, and finally aqueous species, $Si(OH)_4$, accompanied by silicon bond breakage, resulting in the slow dissolution of silicon.[34,35,41] A similar mechanism could apply to the oxidation in the $CaCl_2$ melt. Because chloride ion can act as a Lewis base in molten salts [42], it can coordinate with the surface dangling bond of silicon. The formation of this $Si–Cl_{ads}$ layer might passivate the silicon surface, with perhaps higher complexes, e.g. $Si–2Cl_{ads}$ and $Si–3Cl_{ads}$ formed with further oxidation, and finally leave the surface as, for example, $SiCl_4$ or a related form. The silicon bond breakage would not be as fast as in HF solution since the polarizing effect of chloride is smaller than that of fluoride. As shown in Fig. 7a, the oxidation peak of Si(1 1 1) is much smaller than that of Si(1 0 0) in $CaCl_2$ melt. This behavior is similar to that observed in an alkaline aqueous solution but different from that observed in HF, where there is little difference between Si(1 0 0) and Si(1 1 1) in the oxidation current and the dissolution rate [34,35]. The Si oxidation rate in a $CaCl_2$ melt is thus limited by the number of active silicon sites exposed to the electrolyte and the rate of the silicon bond breakage as in alkaline solution. The oxidation peak current density (5.8 mA/cm^2 on Si (1 0 0)) here is a little higher than that in alkaline solution. Since the oxidation peak current density in 2 M KOH solution depends on temperature, ~0.4 mA/cm^2 at 25 °C and ~1.6 mA/cm^2 at 65 °C [40], compared to the 5.8 mA/cm^2 in the melt at 850 °C.

To determine the nature of the Si species on the surface formed by oxidation in the melt, XPS analysis was performed on the oxidized silicon wafer (Fig. 8). After oxidizing at 1.2 V vs. Dyn. Ca/Ca^{2+} in the $CaCl_2$ melt for 600 s, the silicon wafer was transferred to XPS chamber without exposure to air. The detailed procedure is described in Section 2. Although the wafer following oxidation and washing was not exposed to air, some native oxide as identified via Si 2p peak at 103.2 eV and an oxygen peak were found in the spectrum, probably due to the result of the presence of a few ppm oxygen and water present in the glove box. In addition, it was difficult to remove the $CaCl_2$ residue completely from the silicon surface so that strong Ca 2p and Cl 2p peaks were also seen in the spectrum. Nevertheless, some silicon 2p peaks in different

oxidation states were found as well as bulk Si and native oxide peaks. The peaks at 100.9 eV and 102.2 eV correspond to Si^{+} and Si^{2+}, respectively [36], which are almost equal to those of $Si–Cl_{ads}$ and $Si–2Cl_{ads}$ compound on a Si wafer [43,44]. This is consistent with our speculation about the oxidation of silicon in the $CaCl_2$ melt.

In summary, during the oxidation of silicon in a $CaCl_2$ melt, the silicon is passivated by chloride ion with the formation of unknown surface compounds, probably involving Cl. The following reduction peak represents the reduction of these silicon–chloride species to silicon with a CV peak suggesting a surface-confined reduction. The amount of charge in the reduction, which is $\sim$20 mC/cm^2, is larger than that of a electroactive surface monolayer (equivalent to a few hundreds μC/cm^2) on the Mo, suggesting roughness of the surface and the true area becoming larger with the formation of pores on the surface as shown in Fig. 7b. The charge associated with the reduction peak was about 90% of that of the oxidation peak, indicating that roughly 10% might be related to the formation of a soluble or gaseous by-product. $SiCl_4$ in $CaCl_2$ melt did not generate a distinct reduction peak in CV when it was directly introduced into the $CaCl_2$ melt with Ar carrier gas through an alumina tube (Fig. S4 in the Supporting information). A moderate bubbling of $SiCl_4$ did not cause any change in the CV on Mo in a pure $CaCl_2$ melt, indicating that $SiCl_4$ probably did not dissolve to an appreciable level in the melt. Although vigorous bubbling of $SiCl_4$ resulted in a very noisy CV, a reduction peak did not appear in the first scan. Actually, a very small amount of a silicon deposit (<4 at.% from EDS analysis) was obtained on the Mo surface during this experiment, presumably due to the reduction occurring at more negative potentials from gas phase $SiCl_4$. This reduction led to generation of a Si oxidation peak in the reverse sweep and a re-reduction peak in the next scan.

4. Conclusions

A silicon layer was obtained by reducing SiO_2 NPs in 850 °C $CaCl_2$ molten salt. The CVs on a Mo electrode show an irreversible current for the reduction of SiO_2 NPs and the generation of a new redox couple at more positive potentials that is characteristic of silicon in a $CaCl_2$ molten salt. This couple involves surface species, probably with the Si complexed with chloride ion. The silicon deposit obtained was not a continuous film, but it was in pure elemental state and crystalline. No photocurrent was found with these films, however.

Acknowledgments

We appreciate financial support of this project from the Dow Corning Corporation, the Robert A. Welch Foundation (H-F-0037) and the Center for Electrochemistry.

Appendix A. Supplementary data

Supplementary data associated with this article can be found, in the online version, at doi:10.1016/j.electacta.2012.01.008.

References

[1] D. Elwell, R.S. Feigelson, Solar Energy Mater. 6 (1982) 123.
[2] A.K. Agrawal, A.E. Austin, J. Electrochem. Soc. 128 (1982) 2292.
[3] J. Gobet, H. Tannenberger, J. Electrochem. Soc. 133 (1986) C322.
[4] J.P. Nicholson, J. Electrochem. Soc. 152 (2005) C795.
[5] S.Z.E. Abedin, N. Borissenko, F. Endres, Electrochem. Commun. 6 (2004) 510.
[6] N. Borisenko, S.Z.E. Abedin, F. Endres, J. Phys. Chem. B 110 (2006) 6250.
[7] R. Al-Salman, S.Z.E. Abedin, F. Endres, Phys. Chem. Chem. Phys. 10 (2008) 4650.
[8] T. Munisamy, A.J. Bard, Electrochem. Acta 55 (2010) 3797.
[9] U. Cohen, J. Electron. Mater. 6 (1977) 607.
[10] G.M. Rao, D. Elwell, R.S. Feigelson, J. Electrochem. Soc. 127 (1980) 1940.
[11] D. Elwell, G.M. Rao, Electrochim. Acta 27 (1982) 673.
[12] R. Boen, J. Bouteillon, J. Appl. Electrochem. 13 (1983) 277.
[13] I.G. Sharma, T.K. Mukherjee, Metall. Trans. B 17B (1986) 395.
[14] E.J. Frazer, B.J. Welch, Electrochim. Acta 22 (1977) 1179.
[15] D. Elwell, Solar Energy Mater. 5 (1981) 205.
[16] T. Nohira, K. Yasuda, Y. Ito, Nat. Mater. 2 (2003) 397.
[17] K. Yasuda, T. Nohira, K. Amezawa, Y.H. Ogata, Y. Ito, J. Electrochem. Soc. 152 (2005) D69.
[18] G.Z. Chen, D.J. Fray, J. Electrochem. Soc. 149 (2002) E455.
[19] J. Giner, J. Electrochem. Soc. 111 (1964) 376.
[20] K. Ema, Y. Ito, T. Takenaka, J. Oishi, Electrochim. Acta 32 (1987) 1537.
[21] H. Wendt, K. Reuhl, V. Schwarz, Electrochim. Acta 37 (1992) 237.
[22] V.K. Afonichkin, A.L. Bovet, V.V. Ignatiev, A.V. Panov, V.G. Subbotin, A.I. Surenkovc, A.D. Toropov, A.L. Zherebtsov, J. Fluorine Chem. 130 (2009) 83.
[23] W.F. Linke, Solubilities, Inorganic and Metal-Organic Compounds; a Compilation of Solubility Data from the Periodical Literature, 4th ed., Van Nostrand, Princeton, NJ, 1958, p. 596.
[24] S. Shaw, R. Watson, in Abstract 2999, The Electrochemical Society Meeting Abstracts, Vol. 2008, Honolulu, Hawaii, Oct. 12–17, 2008.
[25] K. Dring, R. Dashwood, D. Inman, J. Electrochem. Soc. 152 (2005) E104.
[26] K. Yasuda, T. Nohira, Y.H. Ogata, Y. Ito, J. Electrochem. Soc. 152 (2005) D208.
[27] W. Xiao, X. Jin, Y. Deng, D. Wang, G.Z. Chen, J. Electroanal. Chem. 639 (2010) 130.
[28] T. Nakagawa, N.S. Bjorge, R.W. Murray, J. Am. Chem. Soc. 131 (2009) 15578.
[29] J.K. Srivastava, M. Prasad, J.B. Wagner, J. Electrochem. Soc. 132 (1985) 955.
[30] X. Jin, P. Gao, D. Wang, X. Hu, G.Z. Chen, Angew. Chem. Int. Ed. 43 (2004) 733.
[31] E. Juzeliunas, A. Cox, D.J. Fray, Electrochem. Commun. 12 (2010) 1270.
[32] D. Laser, A.J. Bard, J. Phys. Chem. 80 (1976) 459.
[33] L.C. Burton, A.H. Madjid, Phys. Rev. 185 (1969) 1127.
[34] X.G. Zhang, Electrochemistry of Silicon and Its Oxide, Kluwer Academic Publishers, New York, 2004, p. 353.
[35] L. Volker, Electrochemistry of Silicon; Instrumentation, Science, Materials and Applications, Wiley-VCH, 2002, p. 51.
[36] E.K. Propst, P.A. Kohl, J. Electrochem. Soc. 141 (1994) 1006.
[37] M.M. Rieger, P.A. Kohl, J. Electrochem. Soc. 142 (1995) 1490.
[38] M. Christophersen, J. Carstensen, A. Feuerhake, H. Föll, Mater. Sci. Eng. B 69 (2000) 194.
[39] E.D. Palik, H.F. Gray, P.B. Klein, J. Electrochem. Soc. 130 (1983) 956.
[40] E.D. Palik, O.J. Glembocki, J.D. Rinko, J. Electrochem. Soc. 136 (1989) 1420.
[41] P. Allongue, V. Costa-Kieling, H. Gerischer, J. Electrochem. Soc. 140 (1993) 1018.
[42] M. Fleischmann, D. Pletcher, J. Electroanal. Chem. 25 (1970) 449.
[43] L.J. Whitman, S.A. Joyce, J.A. Yarmoff, F.R. McFeely, L.J. Terminello, Surf. Sci. 232 (1990) 297.
[44] C.C. Cheng, K.V. Guinn, V.M. Donnelly, I.P. Herman, J. Vac. Sci. Technol. A 12 (1994) 2630.